

# Probing the magnetic fields of massive star forming regions with methanol maser polarisation

R. Dodson<sup>1\*</sup>, C. D. Moriarty<sup>1</sup>

<sup>1</sup> *International Centre for Radio Astronomy Research, Perth, Australia*

Accepted . Received .

## ABSTRACT

Methanol masers can provide valuable insight into the processes involved in high-mass star formation, however the local environment in which they form is still unclear. Four primary, yet conflicting, models have emerged to explain the commonly observed methanol maser structures at 6.67 GHz. These suggest that masers trace accretion disks, outflows, shock fronts or disks dominated by infall/outflows. One proposed means of testing these models is through mapping the local magnetic field structures around maser sources, which were predicted to lie parallel to shock and outflows and perpendicular to accretion disks. To follow up this suggestion we have determined magnetic field directions from full polarisation observations of 10 6.67-GHz sources. We find morphology that is parallel to the source structure, indicative of shocks or outflows, in five sources and perpendicular morphology indicative of disks in three. These results do not support any of the expected models and the diverse morphologies observed indicate that the masers could be emitting from different evolutionary stages or environments, or from a common local environment with complex associated magnetic fields. To resolve this conflict we suggest a new approach that will search the simulations of massive star formation, which are just becoming available, for suitable sites for maser emission.

**Key words:** masers: methanol – polarisation – stars: formation – magnetic fields.

arXiv:1201.1687v1 [astro-ph.GA] 9 Jan 2012

\* E-mail: richard.dodson@icrar.org

## 1 INTRODUCTION

The processes involved in high-mass star formation remain the subject of significant ongoing debate. In particular, it is unclear whether the accretion model currently accepted for lower mass stars ( $<8 M_{\odot}$ ) is still applicable at higher masses, or whether an alternate mechanism is required. For massive stars the accretion-disc model becomes more complex, as radiation pressure produced by the protostar becomes theoretically large enough to halt the gravitational inflow of matter before the final mass of the star is achieved (Zinnecker & Yorke 2007). The current models of massive star formation (MSF) are difficult to verify due to the relative scarcity of high-mass star forming regions and the fact that many are obscured by dense surrounding molecular clouds, preventing direct observation. One means of probing these sources is through studies of their radio emission emitted by the molecular clouds surrounding the central site. 6.67-GHz methanol masers are an abundant and intense maser species known to be associated with sites of high-mass star formation (Minier et al. 2005). This makes them ideal probes of the processes at work in their environment.

Current methanol maser studies have focused on the conflicting theories regarding local maser environment. By determining whether methanol masers can be associated with accretion disks, or potentially other star formation mechanisms, they can illuminate the high-mass star formation debate. Studies by Norris et al. (1993, 1998) suggested that the observed linear spatial distributions and velocity gradients of methanol maser features across a source were tracers of rotating accretion disks, which was considered strong evidence that the accretion disks underpinned high-mass star formation. This theory has been further supported through more recent work by Pestalozzi et al. (2004) (on NGC7538) and Moscadelli et al. (2011) (on IRAS 20126+4104). Surcis et al. (2011) has recently advanced a variation of the model for NGC7538, which has the masers on the interface between infall and a torus. However, a wide survey by Walsh et al. (1998) found only 36 out of 97 methanol maser sources to be in linear structures, with the remainder being inconsistent with the disk model. Furthermore, the estimates for the central masses that were derived through a radial analysis of the linear methanol masers yielded extremely large and unlikely stellar masses ( $M > 100M_{\odot}$ ) in some cases. Walsh postulated an alternate model to account for the diverse properties of the methanol masers observed in their survey, in which masers are created through the propagation of shock fronts through molecular clouds. Dodson et al. (2004) further suggested that the masers might be occurring as external shocks propagating through a rotating molecular cloud, which would account for the observed linear velocity gradients. However van der Walt et al. (2007) felt that, after considering typical rotation rates of molecular clouds, the shock front model could not account for the small velocity range observed across maser observations. Shock fronts would be expected to propagate at high speeds, which are inconsistent with the observed low velocities across methanol masers. This overlooks the requirement that, to allow for a long line-of-sight coherent velocity path, the shocks must be close to the plane of the sky, which would reduce the observed velocity range. An alternative model that has been suggested is that methanol masers are located within bipolar outflows. The maser emission is in an environment in which water masers are known to be produced (Bartkiewicz et al. 2011), and these can be found to trace bipolar outflows (Moscadelli et al. 2005). Support for the model was found by De Buizer (2003), who observed  $H_2$  emission, and in De Buizer et al. (2009) observed SiO using the JCMT (SiO 6 $\rightarrow$ 5) and ATCA (SiO 2 $\rightarrow$ 1). Both the SiO and  $H_2$  tracers are typically associated with outflows, and tended to be aligned parallel to the methanol maser distributions. However Bartkiewicz et al. (2009) showed that attempts to apply the model by analysing the observed velocities of maser spots led to a cone vertex that would be offset from the central stellar mass. Additionally, although this model accounts for linearly distributed maser spots, the extent of the linear distributions suggest that the outflows associated with them would need to be highly collimated, requiring high velocities, inconsistent with those observed. In their studies Bartkiewicz et al. (2009) find that a significant fraction of the sources they study form rings with only a few of the sources being linear, which they credit to the improved sensitivity of their observations. Their best explanation of the sources is that they arise from masers on expanding and rotating disks.

Several programs of phase referenced VLBI observations of methanol masers are underway, e.g. Sanna et al. (2010a,b), which will determine the kinematics of these sources. Such observations will provide a powerful diagnostic, but require a long observational timespan. Broad-scale magnetic field morphology should provide an immediate test of the models of methanol maser environments. In the accretion model, magnetic fields follow the gravitational collapse of molecular clouds around a protostar and are expected to thread through the resulting accretion disk in an hourglass shape (Lizano et al. 2009). Thus, if linear maser features traced an accretion disk, magnetic field vectors would be expected to appear perpendicular to the major axis. Conversely, linear distributions in both outflows and shock fronts would be expected to lie parallel to the magnetic field vectors. Methanol is a non-paramagnetic molecule, however the application of a strong magnetic field during the pumping process can lead to small fractional linear or circular polarisation. As a result, the polarisation of observed maser radiation can be directly attributed to the influence of a strong and ordered magnetic field across the maser site. Previous methanol maser studies, (e.g. Vlemmings (2006), Dodson (2008), Surcis et al. (2009), Vlemmings et al. (2010)) have found that the magnetic field vectors show an alignment across the source that was not consistent with the disk model. However the sample size of current polarisation analysis has been too small to observe the extent of this discrepancy. Focusing on the polarisation properties of a sample of 10 observed masers at 6.67 GHz, we have obtained estimates of the broad magnetic field morphology at the sites housing maser activity.

## 2 OBSERVATIONS

The data used in this analysis came from four separate observing sessions: 22 September 1999, 25 September 1999, 20-21 November 2002 and 27 December 2008. All data was taken with the Australia Telescope Compact Array (ATCA) using

a 4 MHz bandwidth with 1024 frequency channels, giving a velocity resolution of  $0.2 \text{ km s}^{-1}$ . They were performed with dual linear antenna feeds to allow for full polarisation analysis, with an initial instrumental polarisation of approximately 1%. The ATCA configurations were 6A and 6C, which typically gives a resolution of 1 to 4 arcseconds depending on the declination. The calibration of data was performed using the *Miriad* software package. All pointings had 20 minutes or more of on-source observation per session, and the primary (and bandpass) calibrations were obtained from 30 minutes observations of PKS 1934-638. To achieve good polarisation calibration, high quality calibration solutions are needed for each channel, thus the unusually long bandpass scan. The primary and secondary sources were calibrated as-per the methods outlined in the *Miriad* manual (Sault & Killeen 2008), keeping the leakage solutions from the primaries to provide the most consistent results. The secondary calibrators in the 2008 dataset provided poor gain results, hence the sources from this set used both the gains and leakage solutions from the primary calibrator 1934-638. Further corrections to the modelled antenna gains were made by performing phase self-calibration on the maser sources in each set across the strongest channel. For sources G291.27-0.70 and G345.01+1.79, weak continuum radiation was visible in the spectra after self-calibration, which was removed using the subtraction task UVLIN. The sources were then imaged with  $0.3 \text{ km s}^{-1}$  channels and deconvolved, combining the data for the two 1999 observations, as well as combining the 1999 and 2002 observations of sources G339.88-1.26 and NGC6334F. Velocity channels were fitted with simple models to provide component positions. The deconvolved Stokes I, Q and U spectra were exported for polarisation analysis in *Mathematica*. Plots of the fractional linear polarisation and polarisation angle, with associated errors, were generated, clipping points with low I intensity. A full description of the methods and the data reduction can be found in Moriarty (2009)<sup>1</sup>. All the image cubes had a sensitivity within a factor of 3 of  $0.3 \text{ Jy}$  per channel.

### 3 RESULTS

Before commencing the discussion of the results it is important to consider the relationship of the linear polarisation angle  $\chi$  to the magnetic field direction. The dominant maser emission can be either parallel or perpendicular to the magnetic field lines, depending on the angle between the magnetic field and line of sight. If it is greater (less) than  $\sim 55^\circ$  the vectors are perpendicular (parallel) to the magnetic field (Goldreich et al. 1973). When the masers are highly saturated there are further complications as non-linear effects alter the relationships, such as the fixed proportionality between circular polarization and magnetic field strength. One can deduce the emerging brightness temperature,  $T_b \Delta\Omega$ , from the circular polarisation measurements, but our datasets do not contain that information. Assuming a typical spot size of  $3 \text{ mas}$  and a flux of  $100 \text{ Jy}$  the brightness temperature would be  $3 \times 10^{11} \text{ K}$ . Unless the beaming angle  $\Delta\Omega$  approaches several degrees this implies that the emerging brightness temperature is lower enough to ensure that the maser is unsaturated. Furthermore highly saturated masers are expected to have significantly higher fractional polarisation levels than we have observed and we can therefore conclude that the emission is never sufficiently saturated to change the emitting regime. If the masers arise in a disk seen edge on, as in the model of Norris (1993), the field lines will be perpendicular to the disk, and therefore at  $90^\circ$  to the line of sight. The angle will remain greater than  $55^\circ$  until the axial ratio between the major and minor axes reaches 57%. As can be seen the Figures, none of our targets show such a large ratio. Alternatively if the targets are due to outflows their extended structure would lead one to expect that they and their magnetic fields are not directed towards us. In which case, again, the magnetic field angle will be perpendicular to the observed polarisation angle. Finally if the targets are ring-like structures dominated by outflow or infall rather than rotation the field structure would be in the disk and radial from the centre of mass. In this case observations from above would show a polarisation vector that rotates across the structure. Observed edge-on the angle to the line of sight would be  $90^\circ$  at the extremes and aligned when looking towards the centre of mass. Therefore we have assumed that the angle is greater than  $55^\circ$  in all plots, as in previous work (Dodson 2008; Surcis et al. 2009), and discuss the likelihood of it not being so in the text.

The one region where this may not be correct is around components C and E in the Western cluster of G339.88-1.26, where the polarisation vectors rapidly change by  $90^\circ$  between the two adjacent emission spots. This is more clearly revealed in the VLBI image presented in Dodson (2008).

The morphology of each maser region has been studied through comparison of our estimates of the magnetic field vector directions and the linear direction of the source. To estimate magnetic field vectors in the maser regions from the polarisation results, we rotated the polarisation angle ( $\chi$ ) to account for a galactic magnetic field correction ( $\phi$ ) as well as the assumed  $90^\circ$  angle difference between the polarisation and magnetic field angles. Local galactic rotation measure (RM) model values for each source are from Van Eck et al. (2011) using the directions and lower-limit kinematic distances. These were nearly always small and are listed in Table 1. The RM models are based on a limited number of measurements extrapolated on to the lines of sight for our sources, whereas the masers are in dense high-mass star forming regions that could be expected to show significant deviations from a global model. Nevertheless the model is the best approach we have to find the estimates for the RM, and the corrections are sufficiently small that errors inherent in them will not make a significant contribution. Magnetic field angles  $\theta_B$  for each source were calculated by subtracting the expected RM angle  $\phi$  and rotating to obtain the perpendicular vectors

$$\theta_B = \chi - \phi + 90 \quad (1)$$

<sup>1</sup> <http://ftp.physics.uwa.edu.au/pub/Honours/2009/Theses/Moriarty>

To determine the relationship between the magnetic field angles and the distribution of maser spots,  $\theta_B$  results were mapped against position data for individual velocity features.

### 3.1 Magnetic field morphologies

Once values of  $\theta_B$  had been determined for the individual spots they were compared to the major axis angles of the maser spot distributions ( $\theta_{axis}$ ) and classified based on the angle offset between the two. We divided the results between the two classes. Angle differences closer to parallel ( $|\theta_B - \theta_{axis}| < 45$ ) were classified as parallel, and angles closer to perpendicular ( $|\theta_B - \theta_{axis}| > 45$ ) were classed as perpendicular. Some sources were classified as disordered based on their morphology. Some sources have components that fall under all classifications (e.g. G339.88-1.26), and in these cases the dominant classification was taken. Major axes were determined through lines of best fit, weighted by maser flux, where the addition of the weighting constraint provided the best approximation to a linear axis for the maser sources. The results are presented in Figures 1 through to 10. It should be noted that this simplified classification does not provide a complete description of the often-complex nature of magnetic field morphologies. However, it provides a test of the primary models for the environments that house linear distributions of methanol masers, which have clearly associated perpendicular/parallel expected field vectors. Looking at the overall morphology trends for the ten sources, three of them showed predominantly perpendicular vectors to the maser axes, five displayed parallel vectors and two displayed disordered structure. A table of the associated properties for each source is provided in Table 1, which lists (amongst other parameters) in column 2 the classification based on the individual spots, and in column 8 the offset between the average polarisation vectors and the weighted major axes.

### 3.2 Individual sources

#### G291.27-0.70

G291.27-0.70 is a relatively weak and compact maser, peaking at 39.6 Jy and having an extent of only a few hundred mas. However following the method in Phillips et al. (1998) we were able to fit positions to the velocity channels with sufficient accuracy to map the source. The results are presented in Figure 1, which shows the maser spot positions on the sky, with the polarisation angles (where detected) overlaid, rotated to indicate the magnetic field direction. The  $1-\sigma$  errors define a range of angles, which are indicated with red dashed lines. The fitted major axis is shown with a light solid line, to indicate the relative orientation of the field direction and the source major axis. In addition the velocity spectrum is shown with total and polarized flux densities, the percentage linear polarisation and the polarisation angle, where detected. The magnetic field angles on the plane of the sky of G291.27-0.70 were found to be constant across the source, and lie at  $\theta_B - \theta_{axis} = -51^\circ$  (perpendicular by our definition) to the source major axis. This we would consider consistent with the model of methanol masers tracing an accretion disk. However the small size and velocity dispersion leads to a predicted enclosed mass of only  $0.2 M_\odot$ .

#### G305.21+0.21

The results from G305.21+0.21 are presented in Figure 2 in the same form as for Figure 1. This source displays relatively consistent polarisation angles across the source, parallel to the linear distribution of the maser features. This is inconsistent with the model of methanol masers tracing an accretion disk and provides support for an outflow or shock front model. The linear structure could be described as an ellipse, but the polarisation angle neither shows a sweep with phase around the arc, nor does the polarisation angle show a  $90^\circ$  phase change at the centre. These would be expected if the source was a disk dominated by infall or outflow. The accretion disk model was supported for this source in a study by Walsh & Burton (2006) who found that this source shares similar observational properties with a low-mass star forming region in the accretion phase. They suggested that this source may be in the very early stages of massive star-formation, where the central mass is deeply embedded in the molecular cloud. Although they state that this source may provide evidence that there is a short-lived accretion phase in this early stage of massive star-formation, they were unable to find any direct tracers of accretion processes (Walsh & Burton 2006). De Buizer (2003) detected parallel  $H_2$  emission from this source that would appear to contradict the accretion disk model, instead lending support to the outflow model. However, he also noted that there is a second nearby methanol source, and it is confusing as to which source can be associated with the  $H_2$  emission. The parallel major axis and magnetic field vectors found lend support to De Buizer's association of the emission with an outflow.

#### G309.92+0.47

The results from G309.92+0.47 are presented in Figure 3, in the same form as for Figure 1. The magnetic field morphology of this region is complex; vectors appear to be predominantly perpendicular, but tend towards parallel in the northern cluster (B-E) and feature J. Note that a weak feature A appears at  $-54.2 \text{ km s}^{-1}$  and thus has been clipped from the spectra, but appears in the upper panel plot. A morphology flip of polarisation was noted in a study by Caswell & Vaile (1995), who identified Zeeman pairs in OH maser sources G309.92+0.48 that indicated magnetic fields in opposite directions in this associated region. This could be associated with components B-E compared to the other features, but we note that the polarisation angle changes smoothly across the source. It is unclear whether the same field as for the OH would be affecting the methanol masers, which may be offset from the OH emission. The maser features themselves appear in an arc- or ring-like

distribution similar to those identified by Bartkiewicz et al. (2009). however the polarisation angles do not show a jump such as which would occur if the angle between the line of sight and magnetic field vector passed through  $\sim 55^\circ$ . This source was originally considered to be a strong candidate for the disk model, however De Buizer (2003) found no evidence of  $H_2$  emission perpendicular to the masers as would be expected in this case. Although our field vectors support the disk model for some features, generally it is not consistent. Our results also contradict a shock or outflow model, where they would be expected to trace the emission. It is possible they could lie in a region with variable magnetic fields.

### **G310.13+0.75**

The results from G310.13+0.75 are presented in Figure 4, in the same form as for Figure 1. G310.13+0.75 is another relatively weak source, peaking at 69.5 Jy. Whilst four velocity features are identifiable these do not display a clear linear distribution, hence it is difficult to associate a linear axis with this source. The polarisation angles found vary across a 40 degree angle range, leading to a confused magnetic field morphology for the source. No previous studies of the source were available to consider additional properties of the region and this source has been classified as possessing disordered structure. It is possible that this could be a combined torus and outflow source.

### **G316.64-0.08**

The results from G316.64-0.08 are presented in Figure 5, in the same form as for Figure 1. The magnetic field vectors are aligned parallel to a linear axis as ruled through components A through I. Two additional weaker components J and K have been excluded from the position map, as they appear offset from the primary cluster by  $\sim (-0.22, 0.25)$  arcseconds and may represent a separate emitting region, complicating the linear fit. Component H shows an angle perpendicular to the magnetic field trend, however the low fractional polarisation ( $< 2\%$ ) could be affecting the accuracy of this angle measurement. Alternatively it could be a region where the line of sight to magnetic field axis crosses  $55^\circ$ . But the varying magnetic field vectors could also indicate the maser clusters may not belong to the same environment and it is possible that there may be more than one stellar mass in the region. As the central cluster displays parallel morphology this may indicate a further example of masers at a shock-front or outflow.

### **G335.79+0.17**

The results from G335.79+0.17 are presented in Figure 6, in the same form as for Figure 1. This source contains a cluster of maser features in a linear distribution, an outlying source consistent with an axis passing through this cluster (H, F) and an offset region of weaker maser emission (I, J, K). The magnetic field vectors found for these features emerge parallel to this axis, excluding component I in the weaker cluster that emerges perpendicular to this trend. A similar distribution is seen in 12.2 GHz methanol maser emission at the same site, and Phillips et al. (1998) suggested the linear sources reflect a disk, whereas the weaker features may be in a dense region of an outflow. Although this is consistent with the field vector found for feature I, it is inconsistent with the parallel morphology of the other magnetic field angles. De Buizer (2003) detected  $H_2$  emission parallel to this region, although it was unclear if this could be directly associated with the methanol maser emission. However, parallel  $H_2$  emission is consistent with the magnetic field angles if they in fact trace an outflow. The parallel angles may also indicate consistency with the shock front model. The weaker cluster complicates applying a shock front or outflow model across the region, however these may represent a separate emitting environment or secondary body.

### **G339.88-1.26**

The results from G339.88-1.26 are presented in Figure 7, in the same form as for Figure 1. This source was the subject of a thorough polarisation investigation by Dodson (2008) using VLBI data that provided greater resolution than is available in the datasets studied for this project. The field vectors determined are consistent with those found previously and appear to be predominantly parallel to the maser emission. Features A and C display opposing polarisation vectors to their neighbours, as observed in the VLBI results, which is most likely from the change in the magnetic field line of sight passing through  $55^\circ$  to the observer, and flipping the magnetic field orientation. The agreement of our averaged vectors with the overall trends of the more detailed VLBI vectors supports the credibility of our method as a test for large-scale structure. However, extended observations at the resolution given by VLBI may provide a clearer indication of finer magnetic field structure, which would be a valuable probe of the inconclusive morphologies displayed across our sources. This source has been classified as parallel and combined with the previous results may be considered a candidate for the shock front model.

### **G345.01+1.79**

The results from G345.01+1.79 are presented in Figure 8, in the same form as for Figure 1. G345.01+1.79 consists of maser features in a linear distribution, with a clear velocity gradient along the source, as can also be seen in Norris et al. (1998). The magnetic field morphology across the source is unclear, with vectors F and H emerging parallel to the axis, whereas vectors K, J and L are perpendicular. If this jump was due to the angle of the line of sight to the magnetic field vectors the magnetic

fields would have to be very disordered, and switch from one domain to the other, twice. We have therefore classified it as disordered in Table 1. De Buizer (2003) identified extended infra-red emission offset from the maser site but parallel to their distribution, as well as H<sub>2</sub> emission from the same elongated region. This is indicative of masers distributed in an outflow. This is supported by the relatively high collimation of the maser features, however the disordered magnetic field vectors found are inconsistent with this model. The outflow model also offers no clear explanation for the linear velocity gradient of the source. A further study of this source by Saliı̄ et al. (2003) states that there is extended evidence for shock fronts propagating through this region, possibly due to the interaction of stellar winds from the central mass with the surrounding molecular cloud. The central shocks suggested by Saliı̄ et al (2003) would require the young protostar to have begun emission, which would indicate maser activity at a later evolutionary phase than, for example, the early phase that was suggested for G305.21+0.21 by Walsh and Burton (2006). Again, the magnetic field vectors found do not show consistent support for this model. It should be noted that many of the velocity features for this source displayed low fractional polarisation (<2%), hence it is possible that the magnetic field across this source is weak and disordered, complicating its association with the models being tested.

### NGC6334F

The results from NGC6334F are presented in Figures 9 and 10, in the same form as for Figure 1. NGC6334F consists of two regions offset by 3.5 arcseconds. We found polarisation angles across the strongest maser features of each source that agree with those found by Ellingsen (2002). Within the central region, the magnetic field emerges parallel to the emission, whereas in the NW region the field vectors appear perpendicular to the maser features. A weak feature, N, appears offset to the north of the NW cluster, outside the range of the position map. The entire NGC6334 region is a site of intense star formation activity, with estimates suggesting the site houses 20-30,000 young stars, dozens of which are presumed to be high-mass. The NGC6334F region is associated with an ultra-compact H<sub>2</sub> region believed to be due to a single massive protostar (Feigelson et al. 2009). It is, however, possible that the offset region represents emission around a second system, considering the nature of the NGC6334 complex. Indeed this region of the complex has no signs of 7-mm emission (Carral et al. 1997) indicating that it is significantly younger. The varying morphologies seen could be indicating that the masers are emitting from different local environments. Alternatively, if feature E is considered to be a separate region from A-C, these vectors could be considered perpendicular to their emission suggesting the central and NW regions may both be evidence of masers tracing accretion discs around different stellar masses.

## 4 DISCUSSION

### 4.1 Disk with Outflow or Infall

Bartkiewicz et al. (2009) strongly suggest that methanol masers originate in the disk or torus around a proto- or a young massive star where the kinematics are strongly influenced by outflow or infall. They base these deductions on their discovery of richer structures (arcs and rings) that they uncovered due to the improved sensitivity of their EVN observations. The model of disk dominated by infall/outflow would produce a very clear signature in the polarisation angles. If the masers trace a disk dominated by infall or outflow the magnetic field would be expected to lie in the disc, radially from the centre of mass. If the line of sight to the observer was from above, then the viewing angle would be close to 90° and the magnetic field vectors would be perpendicular to the observed linear polarisation vectors. If the viewing angle was close to edge-on then the angle between the fields and the line of sight would be greater than 55° at the outer edges of the disk and less than 55° close to the centre of mass. The observable outcome would be either in the rotation of the polarisation vectors around the centre if observed from above or, if in an edge-on view, the fields would appear perpendicular to the source structure at the extremities with a 90° flip approaching the centre of mass. We find no indications of this kind of structure in the sources we have observed.

### 4.2 Rotating Accretion Disk model

If the masers trace a rotating accretion disk, which is observed edge on, the magnetic fields would be expected to be perpendicular to the source structure. As the line of sight would be close to 90° the magnetic field vectors would be perpendicular to the polarisation vectors.

Whilst earlier polarisation studies found field vectors that contradicted the accretion disk model, three of our sources have fields that suggest that this model may still be applicable (G291.27-0.70, G309.92+0.47, NGC6334F (NW)). It is possible that, as suggested by Walsh & Burton (2006), accretion disks may be present in the early stages of high-mass star formation but may cease and give way to other processes, for example after radiation pressure from the central star begins to counteract the gravitational forces influencing accretion. This suggestion is compatible to an extent with a recent simulation by Krumholz et al. (2009). They found accretion disks to be present during the early stages of high-mass star formation, but over time these formed secondary stellar bodies that broke up the original disks.

### 4.3 Shock Front Model

If the masers trace shock fronts the magnetic fields would be expected to be parallel to the shock front as the magnetic fields become ‘piled up’ along that front. Shock fronts tend to be observed close to edge-on where there is a significant optical depth (e.g. Hester (1987)), therefore the angle of the field to the line of sight would be close to  $90^\circ$  and the magnetic field vectors would be perpendicular to the polarisation vectors. The parallel fields observed in five of our maser sources are in agreement with such models, but the other five are not.

In Dodson et al. (2004) we suggested externally generated shocks propagating through a rotating cloud could lead to the linear maser distributions and velocity gradients that have been observed. We postulated as a test of this theory that magnetic fields are expected to be found parallel to the major axis of the masers, the genesis of this paper. A similar theory was suggested by Saliu et al. (2003) in a discussion of the source G345.01+1.79, in which shocks were instead occurring at the interface between stellar winds from the central mass and the surrounding molecular cloud. However only half of the sources observed show the predicted structure.

### 4.4 Outflow models

If the masers trace outflows the magnetic fields would align with the material flow, tracing the outflow direction. When these are observed from the side the angle of the field to the line of sight would be close to  $90^\circ$  and the magnetic field vectors would be perpendicular to the polarisation vectors. Alternatively when the outflow is directed towards or away from the observer the angle is less than  $55^\circ$  and the vectors would be parallel.

That there is no dominant field orientation in our maser sources could be compatible with the model of masers located in outflows, as outflows might be expected to have random alignment. On the other hand we would expect outflows pointing close to our line of sight to have a higher differential velocity across the source. There is no obvious relationship between  $\Delta$ velocity and angle  $\theta_B - \theta_{axis}$  as seen in the data presented in Table 1.

It is becoming possible to include outflows in sophisticated simulations for Massive Star Formation, as investigated in Cunningham et al. (2011). These simulations point to a reduction in the radiation pressure on the infalling matter, potentially explaining why Massive Stars can form despite the nominal Eddington limitations. At the same time they predict winds of the order of  $100 \text{ km s}^{-1}$  that are much greater than those seen across the methanol maser sources. Of course there are regions in the simulations where the velocities are much lower and detailed analysis of where the masers may arise would resolve these questions.

### 4.5 Whither now?

As discussed, we observed both perpendicular and parallel morphologies between magnetic field vectors and maser distributions in our sample of sources studied. Although in several cases magnetic field vectors agree with the postulation that methanol masers are tracing accretion disks, the majority of observations cannot be explained by this model. On the other hand the shock models would produce magnetic fields perpendicular to the source structure, but this model has no explanation for the parallel alignments. Outflows could be aligned randomly to the line of sight. They would have magnetic fields perpendicular to the source structure, but the linear polarisation may or may not be perpendicular to the magnetic field, preventing the observation of a single dominant tendency. This is what we have discovered, but this model is not supported by the expectation that the sources aligned parallel would have higher velocities across the source. If masers arise on a disk dominated by infall or outflow, and we observed this from above, we would expect to measure a smooth sweep of polarisation angle around the centre of the source. This is not found. Nor do we see a reversal of the polarisation vectors approaching the centre. This would be expected from such disks observed edge on, due to the change in angle of the line-of-sight and the magnetic fields.

It is possible that this lack of a dominant simple model may be an indication that methanol masers are seen across a range of different evolutionary stages. Alternatively, masers could be forming in environments that cannot be described by simplistic general models, such as the suggestion in Surcis et al. (2011) that the masers form at the interface between a combination of the two models: a torus and an outflow. The former is complicated to test, but the latter we believe can be tackled by simulations.

This is timely as simulations are approaching a useful degree of sophistication. Starting with Banerjee & Pudritz (2007) and then Krumholz et al. (2009) adaptive mesh refinement 3D radiative-hydrodynamic simulations have shown the production of both sustained accretion disks and multiple, lower mass, bodies in a complex interplay as the MSF regions developed. Our simplistic models for magnetic field alignments would not have produced an adequate description of these sources. However these are only simulations and included neither outflows nor magnetic field effects. Outflows have been included the work of Cunningham et al. (2011). Magnetic field effects are included in lower mass stellar formation simulation studies that use Smoothed Particle Hydrodynamics (Price & Bate 2009).

None of these datasets can yet be used directly to identify the regions that would produce maser emission, but approaches exist which can be added to the existing simulations. We propose to analyse new MSF simulations which we are performing, to identify those regions where the pumping occurs and the masing conditions are met. We will be able to compare these predictions to the structures actually observed, and their development with evolution. We will be able to derive (with those simulations which include the magnetic fields) the observed polarisation properties and test the simulations against the

observed reality. The combination of simulations of these complex regions and detailed observations of actual methanol masers offers a solution to the longstanding lack of clarity in the interpretation of methanol maser environments.

In addition new observational data, with reliable Stokes V data, will also be required. Stokes V will allow direct estimates of the emerging brightness temperatures, among other parameters. The improved C-band receivers currently being installed at ATCA will greatly assist in providing this. Furthermore higher resolution observations will allow measurements of the spot sizes and provide the separation of separate components at the same velocities.

## 5 CONCLUSIONS

We have presented an analysis of the polarisation properties of ten 6.67-GHz methanol maser sources observed by the ATCA, mapping the magnetic field against the distribution of maser features. This represents a large increase in the number of methanol maser sources mapped in polarisation at high resolution. We have utilised the observed angles as a test of the theory that linear distributions of methanol masers trace accretion disks in high-mass star forming regions. Whilst three of the sources studied displayed magnetic fields perpendicular to the major axis, as expected from an accretion disk, five sources displayed parallel vectors more consistent with shock fronts or outflows. None of the fields were found to be consistent with disks dominated by infall or outflow. Whilst outflows could produce both perpendicular and parallel alignments, they should also show greater velocity ranges for the latter case, which is not seen.

The sources observed to have magnetic fields parallel to maser distribution agree with previous polarisation studies that similarly found parallel morphologies, which cast doubt on the accretion disk model (Vlemmings 2006; Dodson 2008; Surcis et al. 2009). The appearance of perpendicular vectors in our results may be an indication that methanol masers are being emitted from different environments or different stages of stellar evolution, wherever favourable conditions for maser action occur. Further work will be undertaken to examine whether simulations will be able to explain the observed features.

## ACKNOWLEDGMENTS

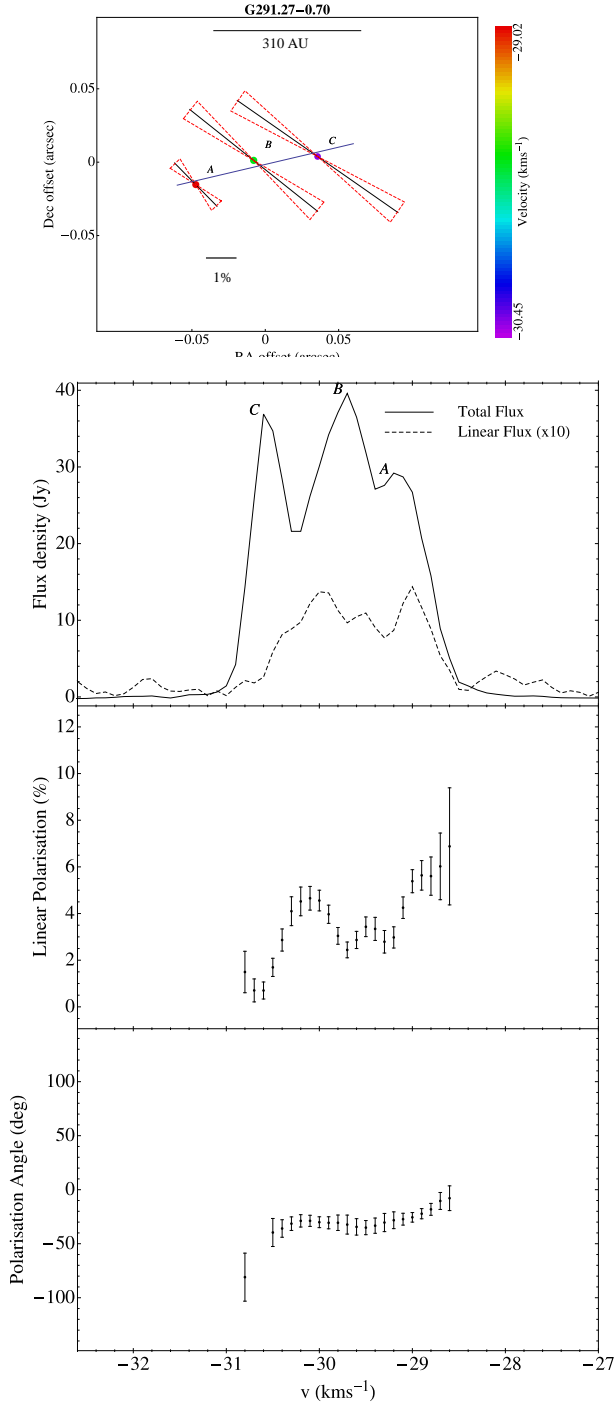
Dr Phillips provided the majority of the maser spot positions from data published in Phillips et al. (1998). Dr Brown and Dr Van Eck provided the solutions for the RM from their model of the Galactic Magnetic field, for each source direction and distance. We are grateful for the comments of the anonymous referee were extremely helpful. The 2008 observations were made under Directors Time at the Australia Telescope for this project. Further data was extracted from the Australia Telescope Online Archive. The Australia Telescope is funded by the Commonwealth of Australia for operation as a National Facility managed by CSIRO.

## REFERENCES

- Banerjee R., Pudritz R. E., 2007, *ApJ*, 660, 479  
 Bartkiewicz A., Szymczak M., Pihlström Y. M., van Langevelde H. J., Brunthaler A., Reid M. J., 2011, *AA*, 525, A120  
 Bartkiewicz A., Szymczak M., van Langevelde H. J., Richards A. M. S., Pihlström Y. M., 2009, *AA*, 502, 155  
 Carral P., Kurtz S. E., Rodriguez L. F., de Pree C., Hofner P., 1997, *The Astrophysical Journal Letters*, 486, L103+  
 Caswell J. L., Vaile R. A., 1995, *MNRAS*, 273, 328  
 Cunningham A. J., Klein R. I., Krumholz M. R., McKee C. F., 2011, *The Astrophysical Journal*, 740, 107  
 De Buizer J. M., 2003, *MNRAS*, 341, 277  
 De Buizer J. M., Redman R. O., Longmore S. N., Caswell J., Feldman P. A., 2009, *AA*, 493, 127  
 Dodson R., 2008, *AA*, 148, 767  
 Dodson R., Ojha R., Ellingsen S., 2004, *MNRAS*, 351, 779  
 Ellingsen S. P., 2002, in *Cosmic Masers: From Proto-Stars to Black Holes Vol. 206 of IAU Symposium, Polarization properties of 6.7 GHz methanol masers in NGC6334F*. V. Migenes and M.J. Reid, 151  
 Feigelson E. D., Martin A. L., McNeill C. J., Broos P. S., Garmire G. P., 2009, *The Astronomical Journal*, 138, 227  
 Goldreich P., Keeley D. A., Kwan J., 1973, *The Astrophysical Journal*, 179, 111  
 Hester J. J., 1987, *The Astrophysical Journal*, 314, 187  
 Krumholz M. R., Klein R. I., McKee C. F., Offner S. S. R., Cunningham A. J., 2009, *Science*, 323, 754  
 Lizano S., Shu F. H., Galli D., Glassgold A., 2009, in *Revista Mexicana de Astronomia y Astrofisica Conference Series Vol. 36 of Revista Mexicana de Astronomia y Astrofisica*, vol. 27, Magnetized disks around young stars  
 Minier V., Burton M. G., Hill T., Pestalozzi M. R., Purcell C. R., Garay G., Walsh A. J., Longmore S., 2005, *AA*, 429, 945  
 Moriarty C., 2009, Master's thesis, University of Western Australia  
 Moscadelli L., Cesaroni R., Rioja M. J., 2005, *AA*, 438, 889  
 Moscadelli L., Cesaroni R., Rioja M. J., Dodson R., Reid M. J., 2011, *AA*, 526, A66  
 Norris R. P., Byleveld S. E., Diamond P. J., Ellingsen S. P., Ferris R. H., Gough R. G., Kesteven M. J., McCulloch P. M., Phillips C. J., Reynolds J. E., Tzioumis A. K., Takahashi Y., 1998, *The Astrophysical Journal*, 508, 275  
 Norris R. P., Whiteoak J. B., Caswell J. L., Wieringa M. H., Gough R. G., 1993, *The Astrophysical Journal*, 412, 222  
 Pestalozzi M. R., Elitzur M., Conway J. E., Booth R. S., 2004, *The Astrophysical Journal*, 603, L113



- Phillips C., Norris R. P., Ellingsen S. P., McCulloch P. M., 1998, MNRAS, 300, 1131  
Price D. J., Bate M. R., 2009, MNRAS, 398, 33  
Salii S. V., Sobolev A. M., Kalanina N. D., Ellingsen S. P., Cragg D. M., Godfrey P. D., 2003, Communication of the Konkoly Observatory Hungary, 103, 75  
Sanna A., Moscadelli L., Cesaroni R., Tarchi A., Furuya R. S., Goddi C., 2010a, AA, 517, A71  
Sanna A., Moscadelli L., Cesaroni R., Tarchi A., Furuya R. S., Goddi C., 2010b, AA, 517, A78  
Sault B., Killeen N., 2008, Miriad User Guide. Australia Telescope National Facility  
Surcis G., Vlemmings W. H. T., Dodson R., van Langevelde H. J., 2009, AA, 506, 757  
Surcis G., Vlemmings W. H. T., Torres R. M., van Langevelde H. J., Hutawarakorn Kramer B., 2011, AA, 533, A47  
van der Walt D. J., Sobolev A. M., Butner H., 2007, AA, 464, 1015  
Van Eck C. L., Brown J. C., Stil J. M., Rae K., Mao S. A., Gaensler B. M., Shukurov A., Taylor A. R., Haverkorn M., Kronberg P. P., McClure-Griffiths N. M., 2011, The Astrophysical Journal, 728, 97  
Vlemmings W. H. T., 2006, MNRAS, 371, L26  
Vlemmings W. H. T., Surcis G., Torstensson K. J. E., van Langevelde H. J., 2010, MNRAS, 404, 134  
Walsh A. J., Burton M. G., 2006, MNRAS, 365, 321  
Walsh A. J., Burton M. G., Hyland A. R., Robinson G., 1998, MNRAS, 301, 640  
Zinnecker H., Yorke H. W., 2007, Ann. Rev. Aston. Astroph., 45, 481

**Figure 1.**

Top) The map of the maser emission for G291.27-0.70, relative to 11:11:53.37 -61:18:23.50 with the integrated features labeled with letters and, where polarized emission was detected, overlaid with the magnetic field direction scaled by the linear polarized flux. One  $\sigma$  errors are indicated and the lower horizontal bar provides the scale for 1% linear polarisation. The spot colour indicates the velocity and the light solid line indicates the best fit axis to the maser features. The upper horizontal bar provides a scale in AU, using the distances we have adopted and listed in Table 1. Bottom) The velocity spectra of the masers, with the integrated features labeled with letters. The top panel is the total flux density and the linear polarized flux density, scaled-up by a factor of 10. The measured fractional linear polarisation, and one sigma errors are shown in the middle panel. The derived polarisation angle  $\chi$ , with one sigma errors, is shown in the bottom panel.

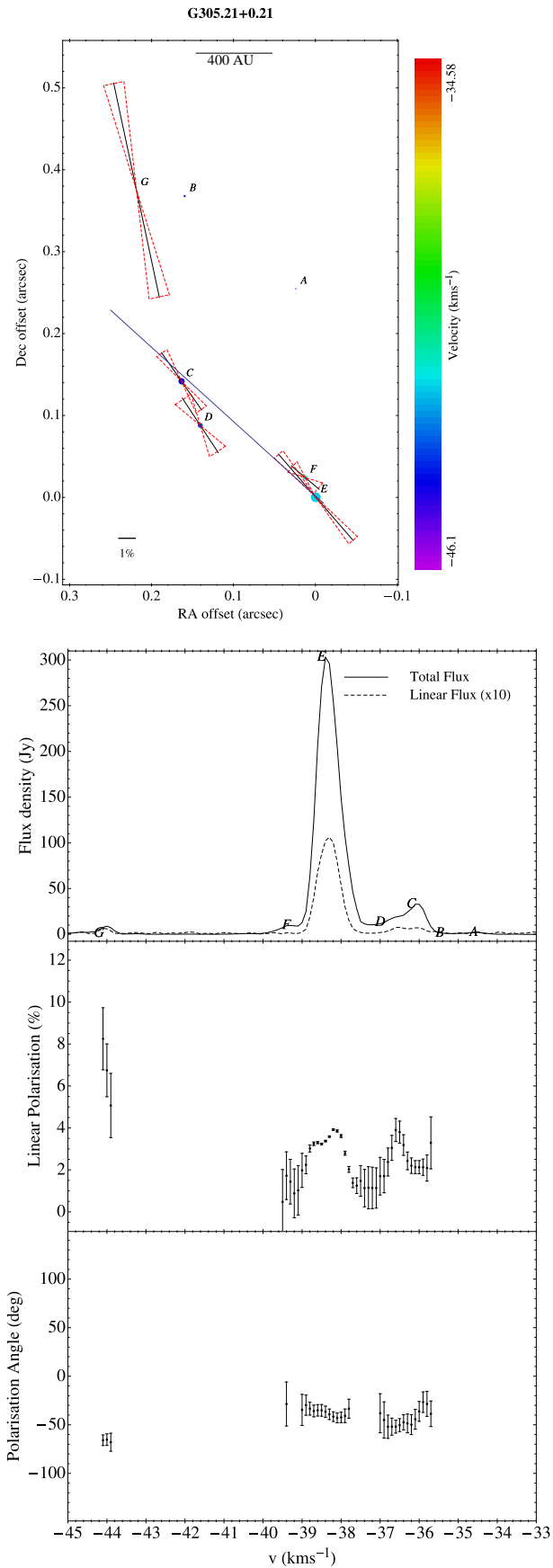


**Figure 2.** As before, for G305.21+0.21, relative to 13:11:14.4 -62:34:26

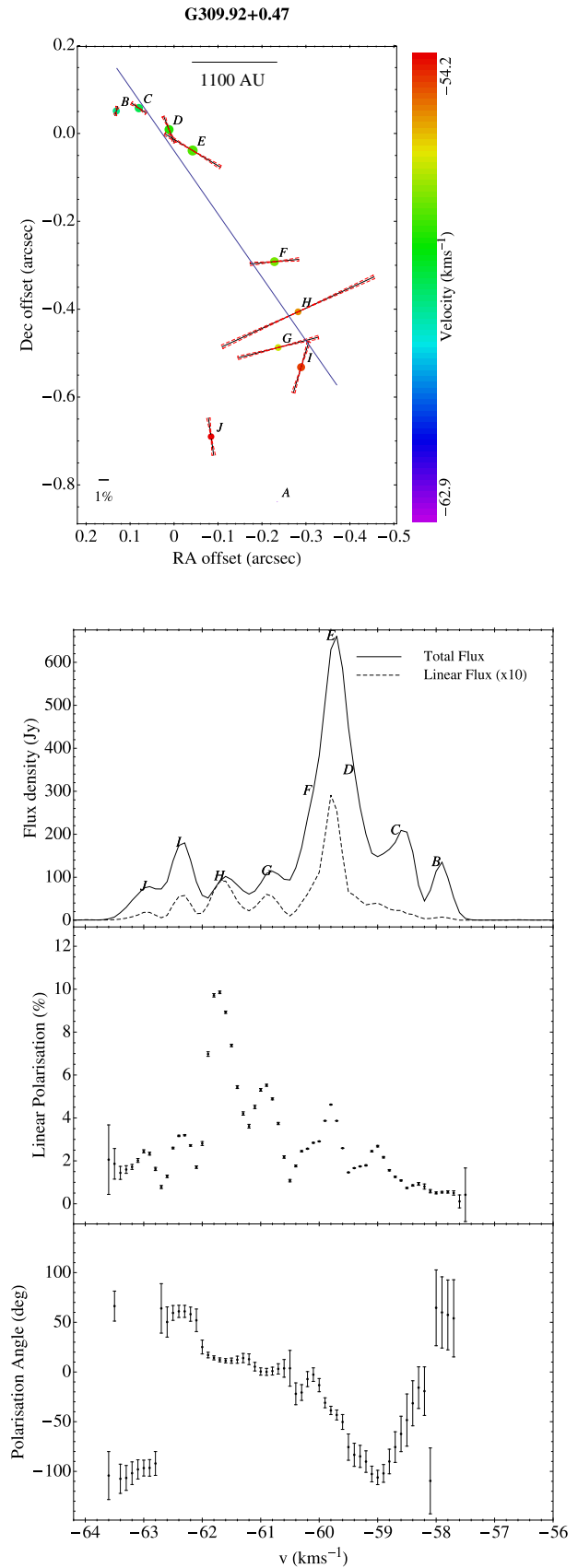


**Figure 3.** As before, for G309.92+0.47, relative to 13:50:41.85 -61:35:11

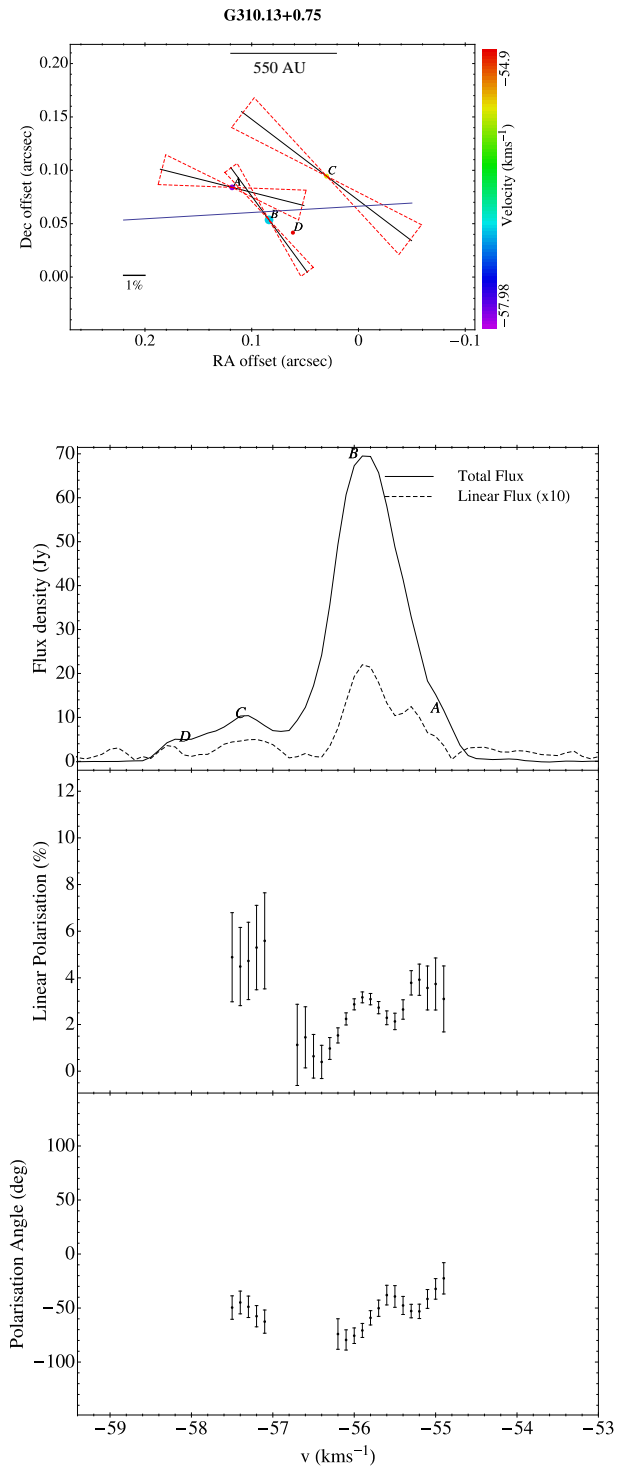


**Figure 4.** As before, for G310.13+0.75, relative to 13:51:54.2 -61:16:18

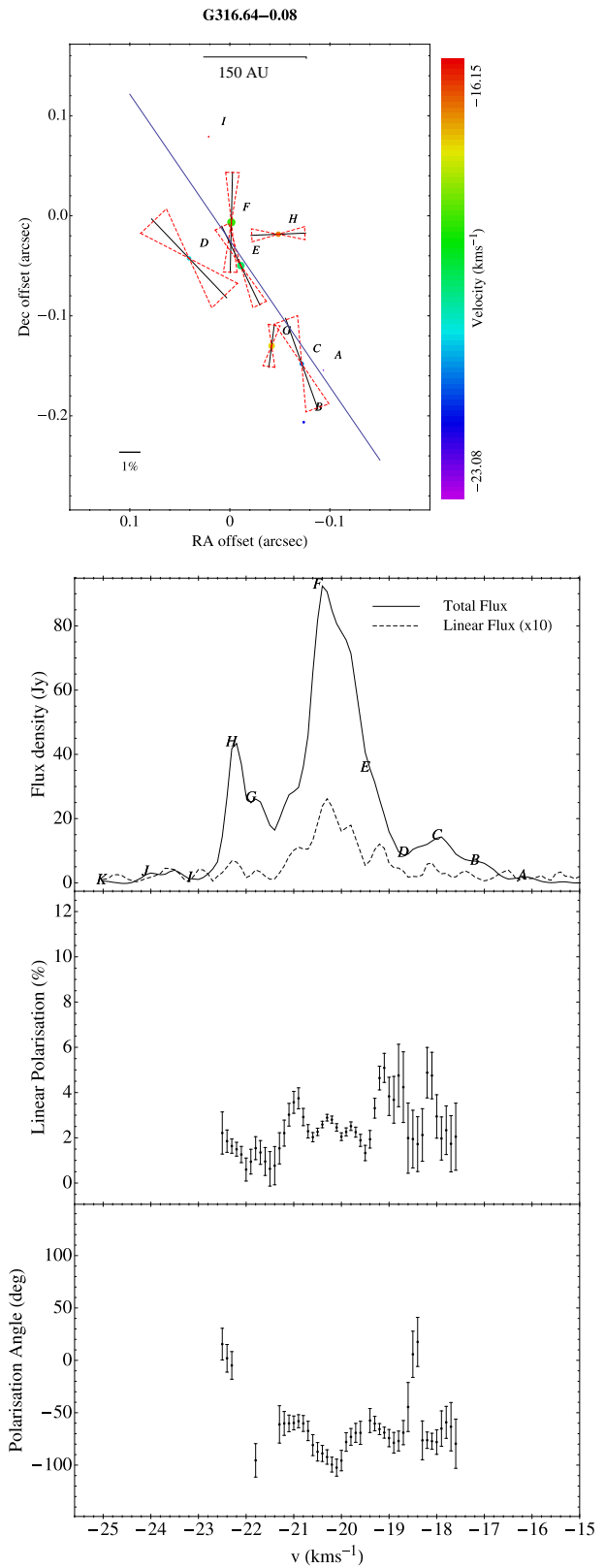


**Figure 5.** As before, for G316.64-0.08, relative to 14:44:18.43 -59:55:12

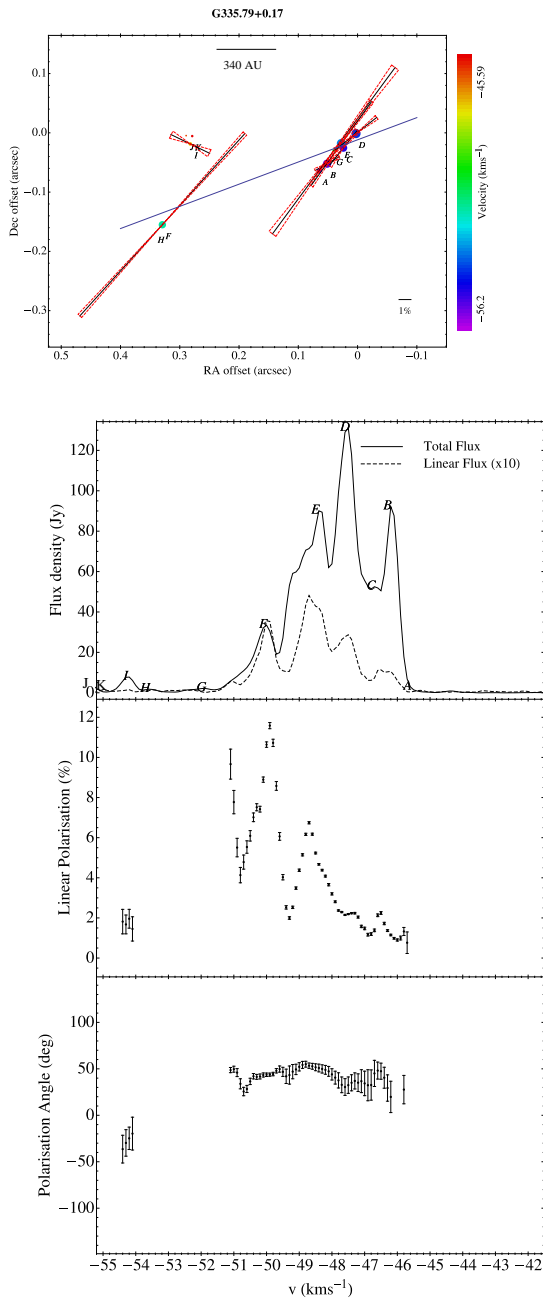


**Figure 6.** As before, for G335.79+0.17, relative to 16:29:47.33 -48:15:52.4

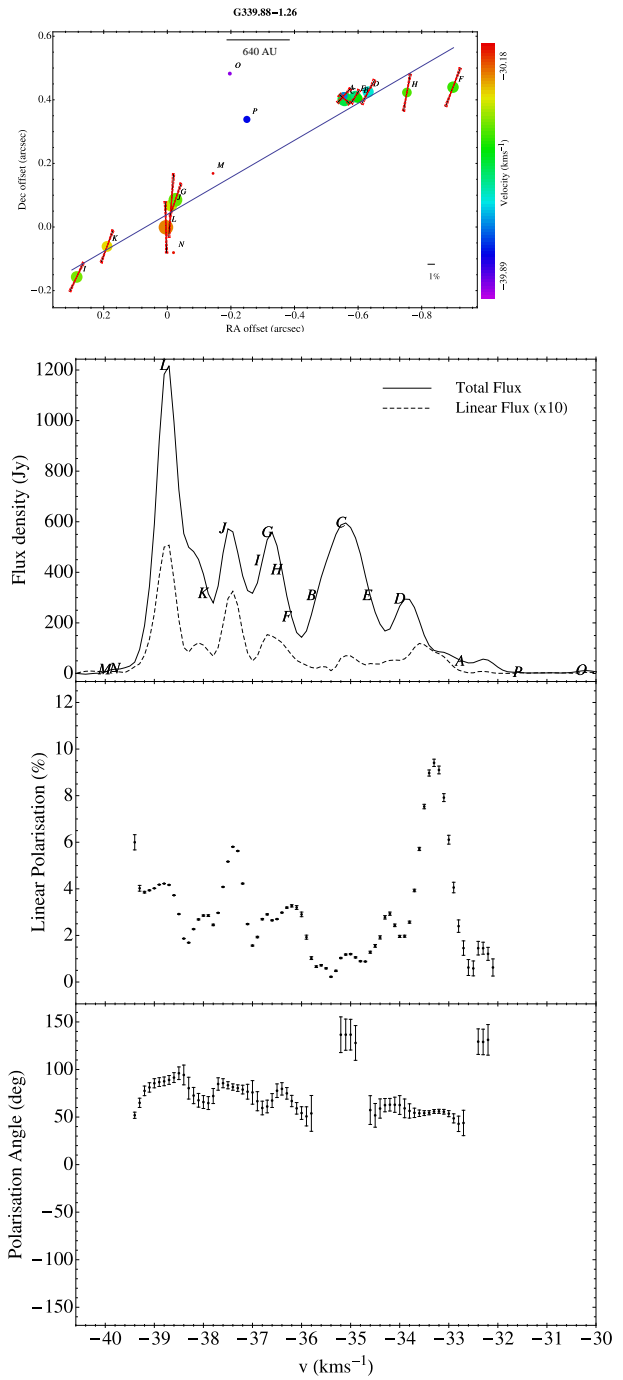


**Figure 7.** As before, for G339.88-1.26, relative to 16:52:04.68 -46:08:34.4

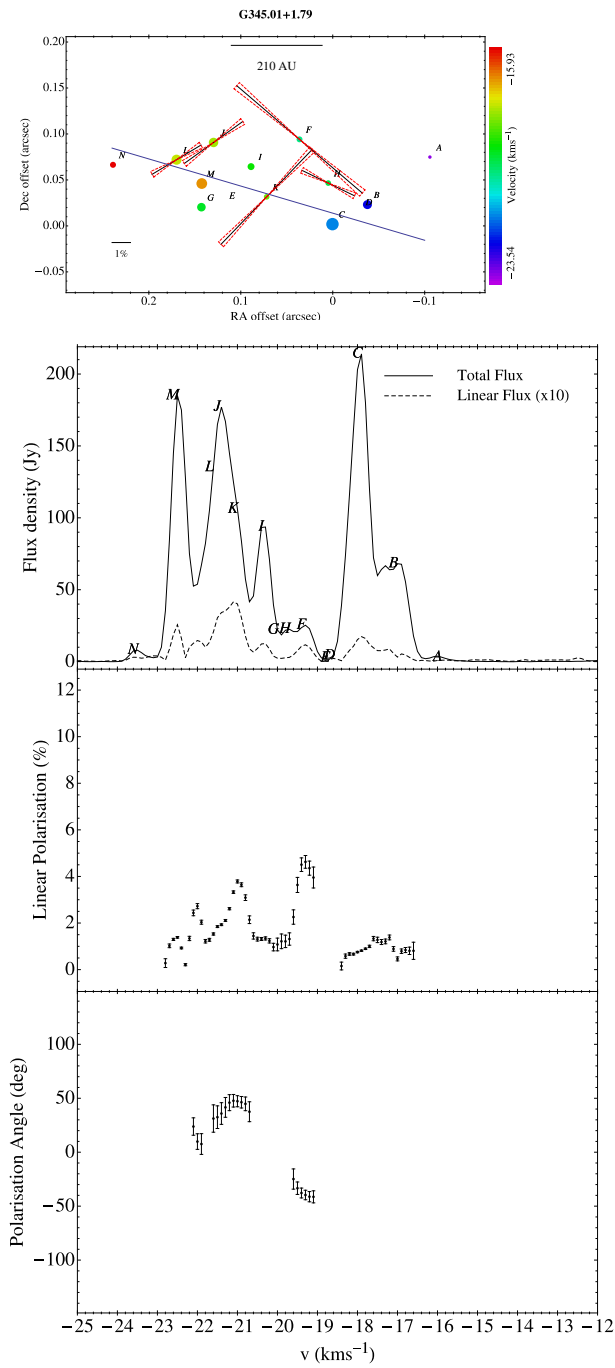


**Figure 8.** As before, for G345.01+1.79, relative to 16:56:47.58 -40:14:25.9

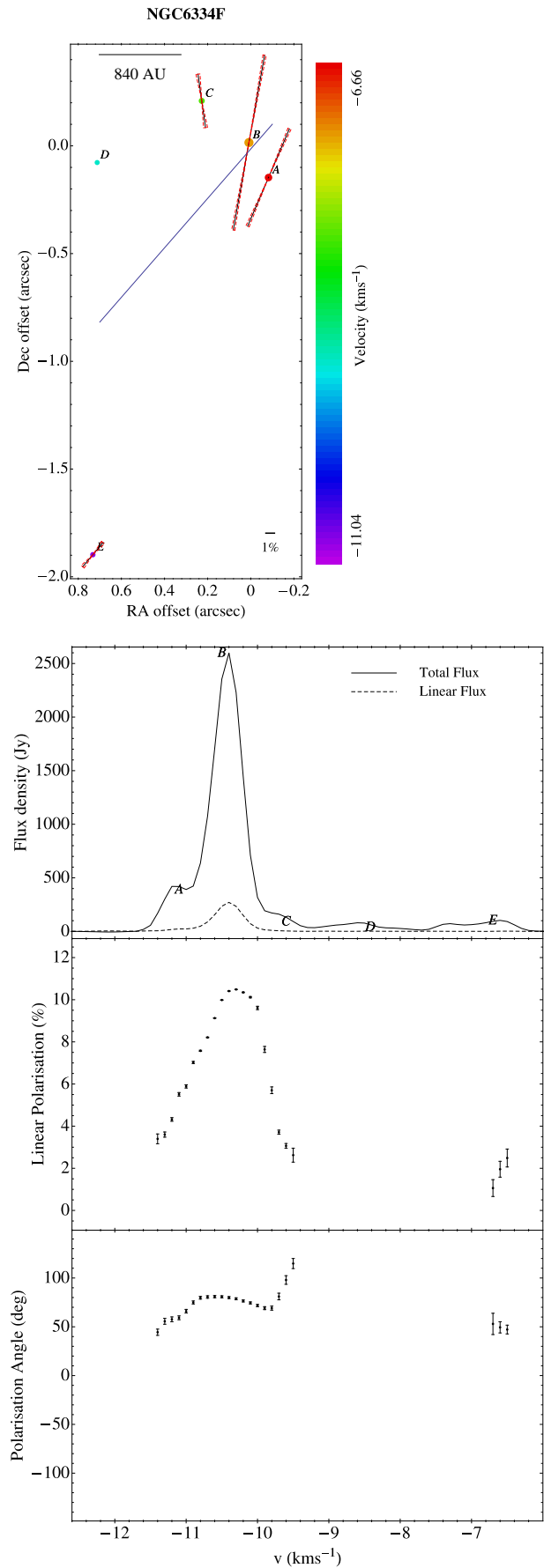


**Figure 9.** As before, for NGC6334F (central), relative to 17:20:53.45 -35:47:00.5 © 0000 RAS, MNRAS 000, 000–000

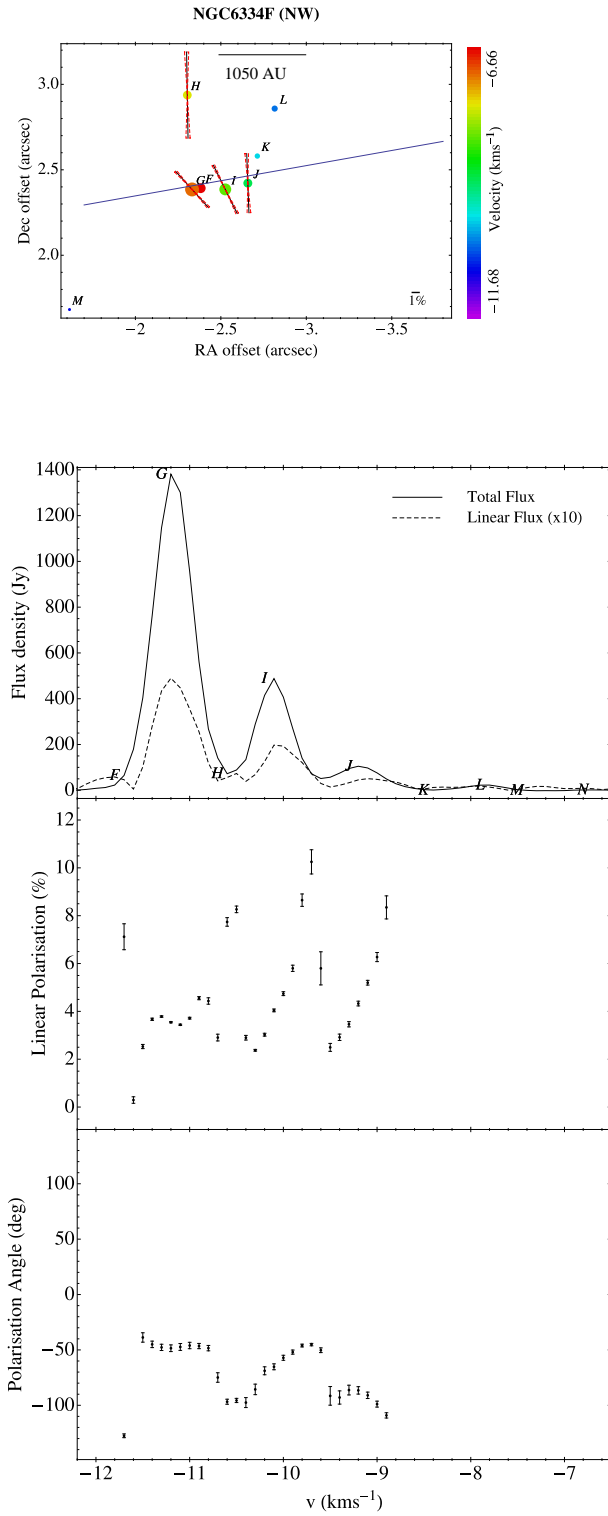


**Figure 10.** As before, for NGC6334F (NW), relative to 17:20:53.45 -35:47:00.5

Name	Classification	Flux (Jy km s <sup>-1</sup> )	Axis $\theta_{axis}$ (deg)	Av. pol. angle $\chi$ (deg)	$V_{lsr}$ (km s <sup>-1</sup> )	Distance (kpc)	RM (rad m <sup>-2</sup> )	Offset $\theta_B - \theta_{axis}$ (deg)	Linear Size (AU)	$\Delta$ velocity (km s <sup>-1</sup> )
G291.27-0.70	perpendicular	40	-77	-32±5	-29.5	3.1	51.1	-51	0.6	2.9
G305.21+0.21	parallel	190	48	-51±14	-38	4.0	99.9	-20	1.7	11.5
G309.92+0.47	perpendicular	898	35	2±56	-60	5.5	-112.6	70	4.7	4.9
G310.13+0.75	disordered	81	-	-56±20	-56	5.5	-113.9	-	0.6	3.8
G316.64-0.08	parallel	102	34	-67 ±36	-20.5	1.5	15.8	-13	0.8	8.8
G335.79+0.17	parallel	252	-69	44±28	-48	3.4	-38.4	28	1.3	10.6
G339.88-1.26	parallel	2571	-60	77±24	-39	3.2	-18.3	48	4.3	9.7
G345.01+1.79	disordered	396	74	5±39	-18	2.1	8.4	20	0.8	7.6
NGC6334F (central)	parallel	1587	-41	77±20	-10.5	2.1	-0.4	28	4.7	4.4
NGC6334F (NW)	perpendicular	733	-80	-71±20	-11	2.1	-0.4	-81	4.6	5.0

**Table 1. Parameters of the Methanol Masers:** Column 1 gives the source name. Column 2 our classification based on the orientation of the magnetic field directions of the individual maser components (labeled with letters in the figures) with respect to the major axis of the source. Column 3 gives the integrated flux density (in Jy kms<sup>-1</sup>) across the source. Column 4 gives the fitted major axis to the individual maser components positions. Column 5 gives the averaged polarisation angle (weighed by the errors) for the individual masing components, with the standard deviation around that value. Column 6 gives the local standard of rest velocity of the peak emission of the maser. Column 7 gives the distance used to calculate the RM. Column 8 gives the RM derived from the model of Van Eck and Brown (2010), which is scaled by 0.116 to convert to  $\phi$  in degrees of rotation at 6.67 GHz. Column 9 gives the offset between the major axis and rotated averaged magnetic field direction. Column 10 gives the linear size, derived from the angular extent of the observed emission scaled with the distance. Column 11 gives the range of velocities seen in across the source emission.